Journal of Materials Chemistry B

ROYAL SOCIETY OF CHEMISTRY

PAPER

View Article Online
View Journal | View Issue

Cite this: J. Mater. Chem. B, 2022, 10, 6372

Exploration of biomimetic poly(γ-benzyl-L-glutamate) fibrous scaffolds for corneal nerve regeneration†

Tien-Li Ma,[a] Shang-Chih Yang,[b] Ting Cheng,[b] Mei-Yun Chen,[c] Jo-Hsuan Wu,[d] Shu-Lang Liao,[bc] Wei-Li Chen*[bce] and Wei-Fang Su*[af]

Received 16th June 2022,
Accepted 31st July 2022

DOI: 10.1039/d2tb01250b

rsc.li/materials-b

Poly(γ-benzyl-L-glutamate) (PBG) made biomimetic scaffolds are explored as candidate materials for corneal nerve regeneration and neurotrophic keratopathy treatment. The PBG with built-in neurotransmitter glutamate was synthesized and fabricated into 3D fibrous scaffolds containing aligned fibers using electrospinning. In *in vitro* experiments, primary mouse trigeminal ganglia (TG) cells were used. Immunohistochemistry (IHC) analysis shows that TG cells cultured on PBG have no cytotoxic response for 21 days. Without any nerve growth factor, TG cells have the longest neurite length of 225.3 μm in the PBG group and 1.3 times the average length as compared with the polycaprolactone and no scaffold groups. Also, aligned fibers guide the neurite growth and extension unidirectionally. *In vivo* assays were carried out by intracorneal implantation of PBG on clinical New Zealand rabbits. The external eye photos and *in vivo* confocal microscopy (IVCM) show a low immune response. The corneal neural markers (βIII tubulin and SMI312) in the IHC analysis are consistent with the position stained by glutamate of implanted scaffolds, indicating that PBG induces neurogenesis. PBG exhibits mechanical stiffness to resist material deformation possibly caused by surgical operations. The results of this study demonstrate that PBG is suitable for corneal nerve regeneration and the treatment of neurotrophic keratopathy.

1. Introduction

The cornea is the outermost barrier of the eye that protects the eye from foreign invaders. Its multilayer structure consists of the epithelium, stroma, and endothelium.[1] The unmyelinated end of the trigeminal nerve's ophthalmic branch innervates the cornea and forms a sub-basal plexus under the corneal epithelium. The health of corneal sensory nerves is essential to the refractive and protective functions of the cornea since they function as surface nociceptors that transmit sensory stimuli from the corneal surface to the central nervous system.[2,3]

Numerous ocular and systemic diseases may damage corneal sensory nerves and lead to neurotrophic keratopathy, an entity manifested as an impaired corneal sensation that may lead to epithelial breakdown. Such neurotrophic disease may disrupt corneal epithelial healing after damage, causing corneal ulceration, corneal perforation, and even subsequent visual loss. Notably, some ophthalmic surgeries, including cataract surgery, refractive surgery, and corneal transplantation, also inevitably lead to corneal nerve disruptions and prolonged recovery of normal innervation.[4,5] Although treatments with neurotrophic effects, such as autologous serum and associated blood derivatives,[6] neurotrophic growth factors,[7–9] and bandage soft contact lenses, are available nowadays,[10] their overall effects on neurotrophic keratopathy are still suboptimal.

Recently, artificial cornea developed using biomaterials has been proposed. Collagen-based scaffolds demonstrated the ability to promote intracorneal penetration of corneal nerve after transplantation; however, their weaker mechanical strength is a major concern.[11–13] Electrospun fibrous scaffolds are considered alternatives since they have stronger mechanical strength and biomimetic structure of interconnected pores similar to the extracellular matrix.[14,15] Peptide-based fibrous scaffolds are widely used due to their excellent biocompatibility, diversified amino acid sequence, and satisfactory mechanical

[a] Department of Materials Science and Engineering, National Taiwan University, Taipei, Taiwan. E-mail: suwf@ntu.edu.tw
[b] Department of Ophthalmology, National Taiwan University College of Medicine, Taipei, Taiwan. E-mail: chenweili@ntu.edu.tw
[c] Department of Ophthalmology, National Taiwan University Hospital, Taipei, Taiwan
[d] Shiley Eye Institute and Viterbi Family Department of Ophthalmology, University of California, San Diego, California, USA
[e] Advanced Ocular Surface and Corneal Nerve Regeneration Center, National Taiwan University Hospital, Taipei, Taiwan
[f] Department of Materials Engineering, Ming Chi University of Technology, New Taipei City, Taiwan

† Electronic supplementary information (ESI) available. See DOI: https://doi.org/10.1039/d2tb01250b

properties.[16–18] Peptide-based electrospun fibrous scaffolds made from poly(γ-benzyl-L-glutamate) (PBG) have demonstrated great biocompatibility and biodegradability.[15,19,20] For application in neurodegenerative diseases, the glutamate component of PBG can function as an excitatory neurotransmitter,[21,22] and the ionic conductivity of the acid derivative of PBG was shown beneficial for inducing neurite outgrowth in neuron-like rat pheochromocytoma cells and enhancing the differentiation of induced pluripotent stem cell-derived retinal ganglion cell progenitors.[19,23] Furthermore, the alignment of fibers in PBG fibrous scaffolds can guide neurite outgrowth, which is important for neuron communication reconstruction.[19] As a result, PBG fibrous scaffolds are considered the ideal biomaterials for improving corneal nerve regeneration.

In this study using cultured mouse trigeminal ganglia (TG) cells and a rabbit model, the physicochemical characteristics and mechanical properties of PBG electrospun fibrous scaffolds containing aligned fibers were analyzed, as well as the biocompatibility and neurotrophic ability of PBG. Polycaprolactone (PCL), a commercial biomaterial proven to have good biocompatibility and biodegradability in clinical applications,[24] was used as the comparison in this study. To the best of our knowledge, this is the first study demonstrating the capability of PBG biocompatible fibrous scaffolds to promote corneal nerve regeneration *in vivo*.

2. Experimental section

2.1 Chemicals and antibodies

N,*N*-Dimethylacetamide (DMAC), polycaprolactone (PCL: M_w = 280 kDa, PDI = 1.3), glutaraldehyde, collagenase A, DNase I, goat serum, Triton X-100, dimethyl sulfoxide (DMSO), Hoechst 33 258 dye, thiamylal sodium, and xylazine hydrochloride were purchased from Sigma-Aldrich (St. Louis, MO, USA). Tetrahydrofuran (THF) was purchased from Macron (Allentown, PA, USA). Paraformaldehyde was purchased from EMS (Hatfield, PA, USA). Dulbecco's modified Eagle's medium (DMEM)/F-12, trypsin-EDTA, Antibiotic–Antimycotic, Alexa Fluor 488 (A11039), and 594 (A11005) fluorescent dye-conjugated secondary antibodies were purchased from Thermo Fisher Scientific (Waltham, MA, USA). Ketamine hydrochloride (Imaldene 1000) was purchased from Merial (Lyon, France). Proparacaine hydrochloride (Alcaine) was purchased from Alcon (Puurs, Belgium). The anti-βIII tubulin monoclonal antibody (ab41489) was purchased from Abcam (Cambridge, UK). Anti-SMI312 (837 904) was purchased from BioLegend (San Diego, CA, USA). The antifade mounting medium for fluorescence was purchased from Vector Laboratories (Burlingame, CA, USA).

2.2 Preparation of PBG and PCL fibrous scaffolds with aligned fibers

The electrospinning solution was prepared by dissolving a polymer in a co-solvent that contains tetrahydrofuran (THF) and *N*,*N*-dimethylacetamide (DMAC) which was stirred at room temperature overnight. The polymer solution was then placed in a 5 mL glass syringe on a syringe pump and the needle tip was connected to a high voltage supply. A grounded metal cylinder collector wrapped with aluminum foil was rotated at a speed of 3200 rpm and the aligned fibers were collected into fibrous scaffolds. The horizontal distance between the collector and needle tip is 15 cm. The fibrous scaffolds were prepared on 12 mm diameter cover glasses which were pasted on aluminum foil. The parameters of electrospinning are listed in Table S1, ESI.† The thicknesses of the scaffolds depend on the time of the electrospinning process. The electrospinning time, thickness, and scaffold density of the fibrous scaffolds used in *in vitro* cell and *in vivo* experiments are shown in Table S2, ESI.† The hydrophilicity of the polymer fibrous scaffolds was measured by water contact angle measurement (Model 100SB, Sindatek). The fiber diameters of PBG and PCL scaffolds were determined from SEM images. Poly(γ-benzyl-L-glutamate) (PBG) was synthesized and characterized according to the published literature.[15] The detailed descriptions are provided in the ESI† (Fig. S1). The commercial biopolymer polycaprolactone (PCL) was used as a comparison in this study.

2.3 Measurement of the mechanical properties of the fibrous scaffolds

The mechanical properties of the fibrous scaffolds were measured using the tensile strength of the materials which characterizes the maximum uniform plastic deformation of the material using a texture analyzer (TA. XT Plus C; Stable Micro System). The fibrous scaffolds were cut into 2 cm × 1 cm and stretched in one direction for the tensile test.

2.4 Measurement of the transparency of polymer fibrous scaffolds

The transparency of the PCL and PBG fibrous scaffolds was assessed by placing them over the printed NTUH (National Taiwan University Hospital) logo. The quantified light transmittance was analyzed using an Epoch 2 microplate spectrophotometer [BioTek (Agilent), Santa Clara, CA, USA]. The absorbance of light at several wavelengths was detected from 300 to 700 nm. The % transmittance of light was calculated using the formula: % Transmittance = $10^{2\text{-Absorbance}}$.

2.5 Characterization of the morphologies of cells on fibrous scaffolds

The morphologies of cells grown on fibrous scaffolds were captured by scanning electron microscopy (SEM; JSM-6510, Nova). The samples were fixed with 2.5% (v/v in PBS) glutaraldehyde solution followed by a gradual dehydration process. The samples were immersed in gradiently increased concentrations of ethanol aqueous solutions. Finally, the samples were vacuum-dried and imaged by SEM immediately.

2.6 Culture of mouse trigeminal ganglion cells

The protocol for mouse trigeminal ganglion (TG) cells' primary culture was adopted from a published study.[7,25] Fresh trigeminal ganglia were dissected from Bltw: ICR mouse (BioLASCO, Taipei, Taiwan) (postnatal day 10), cut into small pieces, and digested

with 0.2% collagenase A, 0.25 mg mL^{-1} trypsin, and 0.2 mg mL^{-1} DNase I in DMEM/F-12 solution at 37 °C. The harvested dissociated cells were centrifuged at 200 ×*g* for 5 min and repeated every 30 min until fully digested. The pellet was resuspended in a culture medium and plated at a density of 2.5×10^3 cells cm^{-2} on the polylysine and laminin-coated 24-well culture plate. To culture TG cells on the PCL and PBG fibrous scaffolds, the scaffolds were put into a 24-well culture plate followed by fixation by a sterilized O-ring. The plated fibrous scaffolds were then irradiated by UV light overnight, and TG cells were later seeded at a density of 1×10^4 cells $well^{-1}$ for further analyses.

2.7 Cell viability assay

A live-dead cell imaging kit (Thermo Fisher Scientific; R37601) was used to evaluate the cell viability. In brief, TG cells were incubated with live–dead cell imaging dyes for 10–15 min at 37 °C. The stained cells were then washed and imaged under a fluorescence microscope to determine the live (green) or dead (red) cells.

2.8 Immunocytochemical and immunohistochemical analysis

For immunocytochemical (ICC) studies, we assessed the expression of βIII tubulin and SMI312 in TG cells under different culture conditions. The cells were washed, fixed with 4% paraformaldehyde, and permeabilized with 0.1% Triton X-100. Next, the treated cells were blocked with 2% goat serum and incubated with respective primary antibodies (anti-βIII tubulin, anti-SMI312 antibody) at 4 °C overnight. On the next day, the cells were stained with the corresponding species-specific secondary antibodies which conjugated Alexa Fluor 488 and 594. The Hoechst 33 258 dye was used for fluorescent nuclear counterstain and the stained cells were then mounted with a VECTA SHIELD mounting medium. The expression pattern of markers was observed using an Olympus BX51 microscope with a U-RFLT fluorescence attachment (Olympus, Shinjuku, Tokyo, Japan) that was equipped with the Olympus DP2-BSW software. To perform immunohistochemistry (IHC) analysis, rabbits were euthanized with an intravenous injection of 240 mg kg^{-1} of thiamylal sodium. Rabbit corneas were cut into 10 μm sections after cryopreservation, air-dried, and fixed with 4% paraformaldehyde. The fixed sections were permeabilized with 0.4% Triton X-100 and then blocked with BSA and goat serum. To confirm the localization of the intracorneal biomaterials and the growth of the corneal nerve after surgery, corneal sections were incubated with anti-βIII tubulin (a component of the microtubule network in neurons that can be used as a neuronal marker), anti-SMI312 (a pan-axonal neurofilament marker used against highly phosphorylated mature axons), and *anti*-glutamate (a component of PBG) antibodies at 4 °C overnight and then incubated with Alexa Fluor 488, and 594-conjugated secondary antibody. An Olympus BX51 microscope with a U-RFLT fluorescence attachment (Olympus, Shinjuku, Tokyo, Japan) equipped with the Olympus DP2-BSW software was used for image analysis.

2.9 Characterization of neurite length and orientation

The neurite length was measured from TG cells stained with βIII tubulin and Hoechst 33 258 dye by ICC. The length was measured from the cell body to the neurite end and analyzed using the ImageJ software. 120 neurites in different groups were analyzed. The extent of neurite alignment was defined as the percentage of neurites with an angular orientation within ± 15° from the 0–180° axis shown by immunofluorescence staining.

2.10 Intracorneal implantation of fibrous scaffolds in rabbits

New Zealand albino rabbits (2.0–3.0 kg, 6 months old, males) were used in this study. The protocol of animal care followed the regulation of the Association for Research in Vision and Ophthalmology Statement for the Use of Animals in Ophthalmic and Vision Research. The Committee approved the experimental procedures for Animal Research at the National Taiwan University Hospital. All surgeries were performed under general anesthesia by intramuscular injection of ketamine hydrochloride (Imaldene 1000) (35 mg kg^{-1}) and xylazine hydrochloride (5 mg kg^{-1}) and topical 0.5% proparacaine hydrochloride (Alcaine; Alcon). The right eye of each animal was implanted with the PBG or PCL fibrous scaffolds while the left eye remained unoperated. Intracorneal implantation of the fibrous scaffolds was performed after the creation of an intracorneal pocket with a depth of around 200 μm with a crescent knife. The PBG or PCL fibrous scaffolds measured 4 mm in diameter with a thickness of 50–70 μm were then implanted into the corneal pocket. The corneal entrance was then sutured with 10–0 nylon (Fig. S5A–C, ESI†).

2.11 *In vivo* confocal microscopy (IVCM)

After intracorneal implantation of the biomaterials, rabbit corneas were examined on day 4, day 7, day 14, and day 21. An HRT3 *in vivo* confocal microscope (Heidelberg Engineering GmbH, Heidelberg, Germany) was used to evaluate the microstructure of the corneal cells, implanted scaffolds, and the infiltration of inflammatory cells in different layers with image dimensions of 400 μm × 400 μm and a transverse resolution of 1 μm. After the corneas were topically anesthetized, the carbomer gel (Vidisic; Bausch & Lomb, Rochester, NY, USA) was applied to the corneal surface before the examination. For each cornea, at least 300 good-quality images of all corneal layers were obtained on the central cornea.

2.12 Statistical Analysis

A Kruskal–Wallis H-test was used to count the significant differences between the groups. A P-value < 0.05 means a significant difference between groups, represented by *; a P-value < 0.01 means the difference between groups was highly significant, represented by **; a P-value < 0.001 means there is an extremely significant difference between groups, represented by ***. Differences between groups with a P-value > 0.05 are not statistically significant and are not marked.

3. Results and discussion

3.1 Characteristics of fibrous scaffolds

PBG is a synthesized polypeptide containing a neuron stimulant of glutamate. Fig. 1D shows its chemical structure. The fibrous scaffolds of PBG and PCL were prepared by electrospinning and imaged by SEM (Fig. 1A and B). The commercial PCL biopolymer was considered as the comparison group. For *in vitro* and *in vivo* experiments, some conditions were pre-examined and optimized. The diameter of the fibrous scaffolds was controlled at around 1 μm to provide a good environment for cell attachment.[26] According to the SEM images, the fiber diameter of the PBG scaffold is about 1.1 ± 0.2 μm and the PCL is about 1.1 ± 0.1 μm (Fig. S3, ESI†) which ensures good cell attachment and reduces variability. The scaffold density was also maintained as 30 μg mm^{-3} to have high porosity to let nutrients and metabolic wastes exchange effectively between the fibrous scaffolds and their environment. Two different thicknesses of fibrous scaffolds were adopted for *in vitro* and *in vivo* experiments. For *in vitro* experiments, 5 μm-thick fibrous scaffolds were used to benefit the ingrowth and interconnection of TG cells. As for *in vivo* experiments, 50 μm-thick fibrous scaffolds were used to sustain the handling force during the implantation process. The fibrous scaffolds contain aligned fibers which can guide the growth of neural cells and promote neurite extension effectively. The alignment of PCL and PBG fibrous scaffolds was analyzed and is shown in Fig. S6A, ESI.† The high percentage of alignment observed (80%) indicated that the fibers were well aligned. The water contact angles of PBG and PCL fibrous scaffolds are very similar (PBG: 126.3 ± 1.3°, PCL: 124.5 ± 4.5°) which are shown in Fig. S4, (ESI†) so there is little effect and variation in cell adhesion.

We also measured the mechanical properties of PBG and PCL fibrous scaffolds as shown in Fig. 1C. Young's modulus of PBG was almost four times higher than that of the PCL. The results indicated that PBG fibrous scaffolds were stronger than PCL fibrous scaffolds. The representative stress–strain curves of PCL and PBG fibrous scaffolds are shown in Fig. S2A and B (ESI†). The results show that Young's modulus of the PBG scaffold is higher than that of PCL, while the elongation of PBG is lower than that of PCL. This represents that the polypeptide PBG is stronger than the polyester PCL, but the PCL is more ductile and flexible. The mechanical properties of polymer scaffolds can be affected by their chemical structures. Fig. 1D shows the chemical structures of PBG and PCL. The PBG contains a flat phenyl ring and hydrogen bonds, which make the polypeptide rigid and tough. On the other hand, PCL contains a flexible hydrocarbon unit and no hydrogen bonds, which results in a flexible and soft material.[27] To examine the transparency of PCL and PBG fibrous scaffolds of 5 μm thickness, the images of PBS-immersed and cell culture medium-immersed scaffolds were analyzed. The good visibility of the NTUH (National Taiwan University Hospital) logo shown under the scaffolds demonstrated the satisfactory transparency of both PCL and PBG fibrous scaffolds (Fig. 1E). The quantified data of transmittance are shown in Fig. 1F and G. Both scaffolds exhibit more than 65% transmittance in culture medium over the visible light range of 300–700 nm.

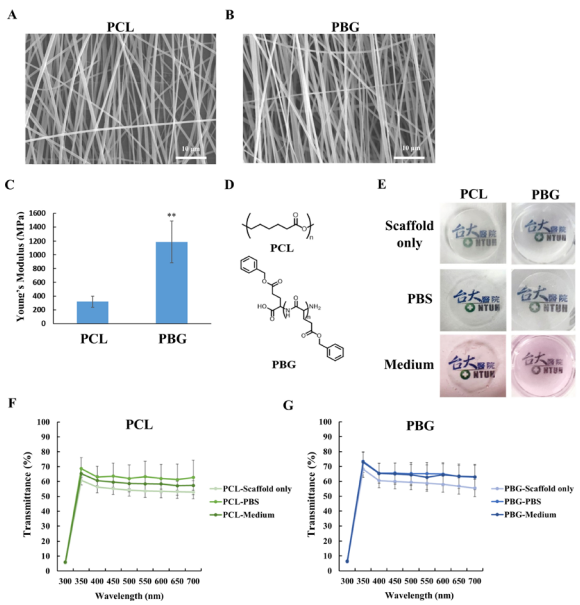

Fig. 1 The SEM images of aligned (A) PCL and (B) PBG fibrous scaffolds for *in vitro* experiments. Magnification: 2000*x*. Scale bar:10 μm (C) Mechanical properties of PCL and PBG fibrous scaffolds. Measurements of each group were repeated 5 times. The Kruskal–Wallis H test: *** represents $P < 0.001$, ** represents $P < 0.01$, and * represents $P < 0.05$. (D) Chemical structures of PCL and PBG. (E) Transparency of PCL and PBG fibrous scaffolds. Both are placed on top of the underneath logo printed on paper and immersed in PBS (Phosphate buffered saline) and a cell culture medium. The transmittance quantification of (F) PCL and (G) PBG over the visible spectrum of the light (300–700 nm) under scaffold only, immersed with PBS and medium.

3.2 *In vitro* biocompatibility assay

To evaluate the biocompatibility of fibrous scaffolds, we collected TG cells and cultured them on different scaffolds. A live/dead assay was performed on day 7, day 14, and day 21. The fluorescence images of the live/dead assay demonstrated more than 90% of live cells in all 3 groups, with significantly greater survival in the PBG group as compared to the PCL group on day 7 (Fig. 2A and B). To further confirm the cell type of the cells that adhered to the fibrous scaffolds, the neural markers βIII tubulin (correlates with neurogenesis) and SMI312 (highly expressed in phosphorylated mature axons) were stained and analyzed on day 21. Expression of the neural markers in the cells was observed in all 3 groups through immunofluorescence imaging (Fig. 2C), suggesting that TG cells can proliferate and express their neuron phenotypes similarly on PCL and PBG fibrous scaffolds. Of note, the directional outgrowth of neurites was observed on both PCL and PBG fibrous scaffolds, but not in the no-scaffold control group (Fig. 2C). The strong expression of mature axons and neurogenesis markers on day 21 also suggested satisfactory maintenance of neural features of the co-cultivated TG cells on PBG fibrous scaffolds (Fig. 2).

3.3 Neurite outgrowth on different fibrous scaffolds

To compare the neurite outgrowth pattern of TG cells on different fibrous scaffolds, immunofluorescence staining of

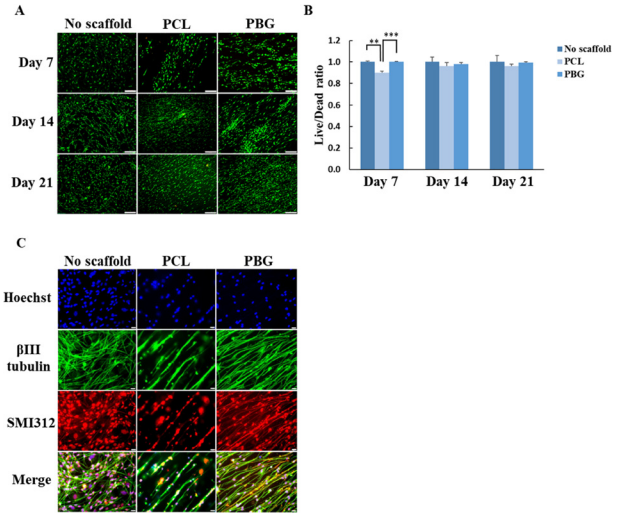

Fig. 2 The biocompatibility and expression of neural markers of TG cells cultivated on PCL and PBG fibrous scaffolds. (A) Representative live/dead fluorescence microscopic images (Scale bar: 200 μm) and (B) Live/Dead ratio of TG cells on day 7, day 14, and day 21. (C) The expression of neural markers of TG cells was examined by the immunocytochemical study 21 days after culture. Green: βIII tubulin. Red: SMI312. Scale bar: 50 μm. The Kruskal–Wallis H test: *** represents $P < 0.001$, ** represents $P < 0.01$, and * represents $P < 0.05$.

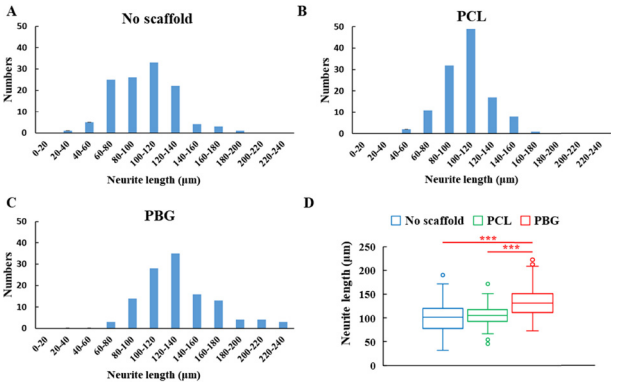

Fig. 3 Distribution of the neurite length of TG cells after 21 days of culture in (A) control (no scaffold), (B) PCL fibrous scaffold, and (C) PBG fibrous scaffold. (D) Box chart of the neurite length distribution in each group. Neurite counts = 120 in each group. The symbol "○" means the outlier of each group. The Kruskal–Wallis H test: *** represents $P < 0.001$, ** represents $P < 0.01$, and * represents $P < 0.05$.

βIII tubulin was used to verify neural cells and analyze the distribution of neurite length on day 21. The neurite length in the no-scaffold and PCL groups was mostly between 100 and 120 μm (Fig. 3A and B), while the neurite length in the PBG group was overall greater, ranging mostly between 120 and 140 μm (Fig. 3C). The box plot of the neurite length in different groups demonstrated that the neurite length in the PBG group was significantly greater than the other two groups, with the longest length being 225.3 μm (Fig. 3D and Table S3, ESI†). A wider distribution of neurite lengths was also noticed in the no-scaffold group, in spite of the shortest average length.

3.4 Alignment of TG neurites

To verify whether TG cells can grow in alignment with the fibrous scaffolds, the distribution of the angular orientation of TG cell neurites was analyzed and shown in an angle distribution map. The results showed that the orientation of TG cell neurites was mostly within 30° from the 0–180° axis degrees when cultured on the PCL/PBG fibrous scaffolds. In contrast, neurites in the no-scaffold control group grew in random orientations (Fig. 4A–C). The extent of alignment of the neurites was almost consistent with that of the fibrous scaffolds (Fig. S6, ESI†). The observations indicated that the neurites of TG cells grow directionally as guided by the fibrous scaffolds. The SEM images of TG cells that grew along with the PCL/PBG fibrous scaffolds are shown in Fig. 4D. The length of neurites in TG cells was significantly longer in the PBG group as compared to that in the no-scaffold and PCL groups. The results suggested that the built-in glutamate neurotransmitter in the PBG fibrous scaffolds can effectively stimulate neurite outgrowth more than none-built-in ones,[15,19] and the single directional alignment of fibrous scaffolds may have a synchronized effect on neural growth (Fig. 3 and 4).

3.5 Intracorneal implantation of PBG fibrous scaffolds in the animal study

To evaluate the intracorneal biocompatibility and neurotrophic ability of the PCL and PBG fibrous scaffolds, they were implanted into the rabbit's cornea interlamellarly respectively. The intracorneally implanted PCL and PBG fibrous scaffolds were well situated in the corneal stroma without causing significant inflammation from day 1 post-surgery to 2 months after the surgery (Fig. S5C–E, ESI†). The external eye photos and IVCM images of PCL and PBG fibrous scaffolds implanted eyes on day 4, day 7, day 14, and day 21 after the surgery are shown in Fig. 5. The results demonstrated no corneal epithelial defects, melting, or infection in both PCL (Fig. 5A) and PBG (Fig. 5B) implanted eyes. The surrounding area of the cornea

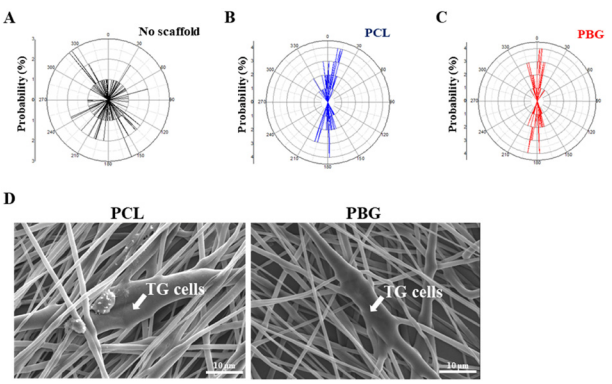

Fig. 4 Orientation of the neurites of TG cells after 21 days of culture on (A) control (no scaffold), (B) PCL fibrous scaffolds, and (C) PBG fibrous scaffolds. Neurite counts = 100–120 in each group. (D) The SEM images of TG cells (arrow) on left: PCL fibrous scaffold and right: PBG fibrous scaffold. The TG cells grew along the fibers of the electrospun fibers. Scale bar: 10 μm.

adjacent to the implanted fibrous scaffolds was transparent. The implanted fibrous scaffolds were well located in the corneal stroma without migration or extrusion. Of note, slow degradation of the implanted PBG fibrous scaffolds was noticed from day 4 to day 21 (Fig. 5B).

The PBG implanted corneas were further examined by IHC 2 months after surgery to evaluate the growth of the corneal nerve on the fibrous scaffolds. The H&E staining of sections showed the existence of an intracorneal scaffold (Fig. 6A). The IHC result showed the co-localization of the corneal nerve (βIII tubulin and SMI312 positive cells) and the implanted PBG fibrous scaffold (Glutamate positive region), which indicated the good neurotrophic/neuro-regenerative ability of the PBG fibrous scaffold that directs the growth of the corneal nerve on them (Fig. 6B and C). In the animal model, the high biocompatibility of the PBG fibrous scaffold was further confirmed. Since the external eye photos and IVCM images showed low immune reactions after intracorneal implantation of PBG in rabbit corneas, there may be less concern about corneal inflammation, melting, infection, or neovascularization for its clinical use. Moreover, with the IHC clearly demonstrating neurogenesis in the implanted scaffolds, the ability of the PBG fibrous scaffold for promoting the regeneration of corneal nerve in clinical applications could be promising (Fig. 5 and 6). In this study, under the same substrate size and dimensions, PBG has nearly four times higher tensile strength than PCL, indicating that PBG has better structural stability and mechanical properties. PBG polypeptide fibrous scaffolds can provide mechanical or biological support structures to promote nerve cell growth, guidance, appropriate targeting, and the maturation and secretion of nerve cells, allowing the normal functioning of biological signaling systems. It can be seen from the *in vivo* animal experiments that the nerve cells perform well after the PBG scaffolds were implanted into the animal for two months. However, PCL is flexible and cannot maintain its structural integrity at 21 days *in vivo* (Fig. S7, ESI†). The PCL-implanted group died after 21 days of the implantation experiment and the observation time for corneal nerve regeneration in animal models is commonly more than 2 months.

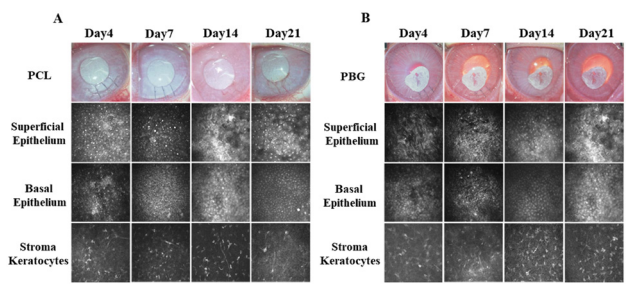

Fig. 5 External eye photos and *in vivo* confocal microscopy (IVCM) images of the (A) PCL and (B) PBG fibrous scaffolds in post-operated eyes on day 4, day 7, day 14, and day 21. For both groups, during the whole observational period, no significant corneal epithelial defect, infiltration, or neovascularization was observed, and IVCM showed normal superficial epithelium, basal epithelium, and stromal keratocytes without significant infiltration of inflammatory cells.

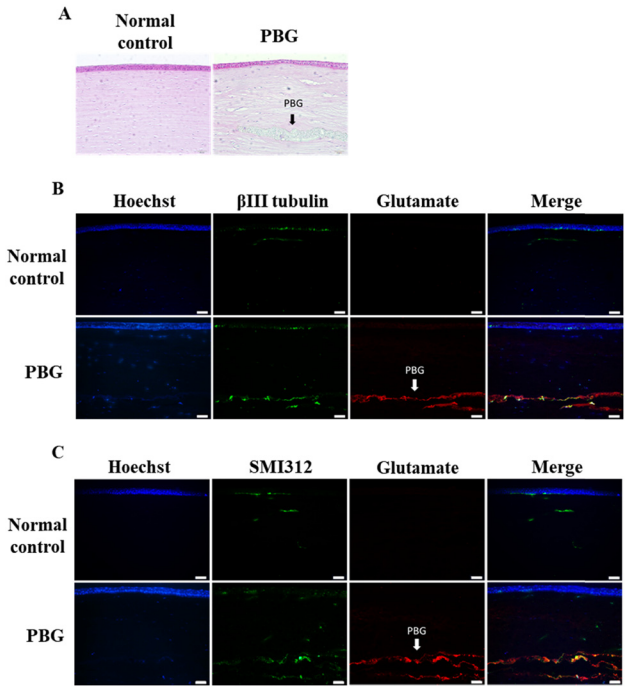

Fig. 6 (A) The histopathological examination of the left (normal) eye and the right (PBG fibrous scaffold implanted) eye after 2 months of surgery. The implanted fibrous scaffold was well located in the corneal pocket without migration causing corneal epithelial defect, inflammation, and melting of neovascularization. The nerve regeneration capability of the PBG fibrous scaffold was examined by neural markers (B) βIII tubulin and (C) SMI312 expression. The PBG fibrous scaffold was identified by glutamate staining. Scale bar: 50 μm.

As a result, the collection time for the PCL-implanted group is not enough to judge the corneal nerve regeneration capability. Furthermore, there is no suitable antibody to recognize PCL which is necessary to demonstrate that the regenerated corneal nerve is co-localized with the PCL scaffold. Although we have performed immunohistochemical analysis of the PCL-implanted group, we cannot judge the corneal nerve regeneration capability of the fibrous PCL scaffold or compare it with the PBG-implanted group parallelly (Fig. S7, ESI†).

The normal innervation of the corneal nerve is essential for maintaining a healthy ocular surface. Damage to the corneal nerve may lead to decreased proliferation of corneal epithelial cells,[28] increased corneal permeability,[29] changes in corneal epithelial phenotypes,[29–31] and delayed wound healing.[29,30] The corneal nerve releases neurotrophic factors, such as calcitonin gene-related peptide, substance P, vasoactive intestinal peptide, and neuropeptide 3, which play important roles in the turnover of the corneal epithelium.[32] The corneal epithelium and keratocyte also release neurotrophic factors, such as brain-derived neurotrophic factor, nerve growth factor, and glial cell-derived neurotrophic factor,[33] which mediate the interaction between the corneal innervation and corneal epithelium and promote corneal epithelial healing and ocular surface homeostasis.

Although topical solutions are the mainstays to promote corneal nerve regeneration at present, as aforementioned, biomaterial scaffolds have emerged as a promising alternative

solution. Biocompatible fibrous scaffolds have been found to promote the proliferation, differentiation, regeneration, and repair of neurons.[34–36] Many synthetic polymers have been studied for nerve regeneration, such as polylactic acid (PLA), polyglycolic acid (PGA), polylactic-*co*-glycolic acid (PLGA), polycaprolactone (PCL) and so on.[37,38] The highly biocompatible polypeptide PBG fibrous scaffold has good mechanical strength and resists the deformation of the transplantation process, and has reproducibility and long shelf life. The novelty of PBG is that it contains glutamate neural stimulant, which has great potential in the field of nerve regeneration.[19,23] This is the first report using PBG-aligned fibrous scaffolds for corneal nerve regeneration. For applications in ophthalmology, biocompatible fibrous scaffolds have also been used for the attachment and proliferation of human limbal stem cells,[39] making them potential alternative carriers in corneal tissue engineering,[40] which may be beneficial for corneal endothelial keratoplasty.[41]

The advantages of peptide-based fibrous scaffolds include not only increased mechanical properties, which make the implantation easier, but they are also biodegradable. The thick PBG fibrous scaffolds that mimic cornea in this study were semi-transparent, and thus the transparency needs to be improved if used clinically. Fabricating scaffolds consisting of a thin diameter of fibers of less than 400 nm without light scattering or by the combination of hydrogels and electrospinning may provide a better solution to improve the light transmission ability of the scaffolds.[42] The possibility of drug-loading and delivery by the scaffolds is another promising strategy to further enhance the effects of fibrous scaffolds in corneal repair,[43] which may be a subject for future study.

4. Conclusions

In this study, the biomimetic poly(γ-benzyl-L-glutamate) (PBG) fibrous scaffolds containing aligned fibers were investigated for corneal nerve regeneration. The results of *in vitro* analyses indicated that the PBG fibrous scaffolds could be safely used as a scaffold for cultivated neuronal cells due to their low cytotoxicity. In addition to the excellent biocompatibility, the ability to guide the directional growth of TG cell neurites is another important characteristic of fibrous scaffolds for future application in corneal nerve regeneration. To the best of our knowledge, no prior studies have demonstrated the *in vivo* neurotrophic effects of electrospun biomaterials in the cornea. The PBG fibrous scaffolds, which can be easily implanted into the cornea without causing a significant inflammatory reaction, showed excellent biocompatibility and the ability to promote corneal nerve regeneration both *in vitro* and *in vivo*. Our results suggest the potential of PBG fibrous scaffolds as good candidates for the clinical treatment of neurotrophic keratopathy.

Author contributions

Tien-Li Ma: data curation, formal analysis, investigation, validation, visualization, and writing – original draft; Shang-Chih Yang: data curation, formal analysis, visualization, and writing – original draft; Ting Cheng: investigation and validation; Mei-Yun Chen: investigation and validation; Jo-Hsuan Wu: writing – review & editing; Shu-Lang Liao: funding acquisition; Wei-Li Chen: conceptualization, funding acquisition, investigation, methodology, project administration, resources, supervision, and writing – review & editing; Wei-Fang Su: conceptualization, funding acquisition, methodology, project administration, resources, supervision, and writing – review & editing.

Conflicts of interest

There are no conflicts to declare.

Acknowledgements

This work was supported by the Ministry of Science and Technology, Taiwan (MOST 108-2221-E-002-027-MY3, MOST 110-2221-E-131-010, MOST 107-2314-B-002-142-MY3, MOST 111-2221-E-002-029) and the National Taiwan University Hospital (NTUH.111-A144). We also thank the staff of the Second Core Lab, Department of Medical Research, National Taiwan University Hospital, for technical support during the study.

Notes and references

1 S. S. Apdavi, M. J. Abdekhodaie, S. Mashayekhan, A. Baradaran-Rafii and A. R. Djalilian, *Tissue. Eng. Regen.*, 2020, **17**(5), 567–593.
2 L. J. Muller, C. F. Marfurt, F. Kruse and T. M. Tervo, *Exp. Eye Res.*, 2003, **76**(5), 521–542.
3 J. He and H. E. Bazan, *Invest. Ophthalmol. Vis. Sci.*, 2016, **57**(2), 664–674.
4 B. H. Lee, J. W. McLaren, J. C. Erie, D. O. Hodge and W. M. Bourne, *Invest. Ophthalmol. Visual Sci.*, 2002, **43**(12), 3660–3664.
5 S. V. Patel, J. C. Erie, J. W. McLaren and W. M. Bourne, *Arch. Ophthalmol.*, 2007, **125**(12), 1693–1698.
6 C. T. Huang, H. S. Chu, K. C. Hung, L. W. Chen, M. Y. Chen, F. R. Hu and W. L. Chen, *Br. J. Ophthalmol.*, 2021, **105**(6), 884–890.
7 S. I. Yeh, S. H. Yu, H. S. Chu, C. T. Huang, Y. P. Tsao, C. M. Cheng and W. L. Chen, *Invest. Ophthalmol. Visual Sci.*, 2021, **62**(1), 23.
8 A. Lambiase, M. Sacchetti and S. Bonini, *Curr. Opin. Ophthalmol.*, 2012, **23**(4), 296–302.
9 N. Yamada, R. Matsuda, N. Morishige, R. Yanai, T. I. Chikama, T. Nishida, T. Ishimitsu and A. Kamiya, *Br. J. Ophthalmol.*, 2008, **92**(7), 896–900.
10 A. Lambiase, P. Rama, L. Aloe and S. Bonini, *Curr. Opin. Ophthalmol.*, 1999, **10**(4), 270–276.
11 C. R. McLaughlin, M. C. Acosta, C. Luna, W. Liu, C. Belmonte, M. Griffith and J. Gallar, *Biomaterials*, 2010, **31**(10), 2770–2778.

12 J. R. Jangamreddy, M. K. C. Haagdorens, M. Mirazul Islam, P. Lewis, A. Samanta, P. Fagerholm, A. Liszka, M. K. Ljunggren, O. Buznyk, E. I. Alarcon, N. Zakaria, K. M. Meek and M. Griffith, *Acta Biomater.*, 2018, **69**, 120–130.
13 C. D. McTiernan, F. C. Simpson, M. Haagdorens, C. Samarawickrama, D. Hunter, O. Buznyk, P. Fagerholm, M. K. Ljunggren, P. Lewis, I. Pintelon, D. Olsen, E. Edin, M. Groleau, B. D. Allan and M. Griffith, *Sci. Adv.*, 2020, **6**(25), eaba2187.
14 D. H. Reneker and A. L. Yarin, *Polymer*, 2008, **49**(10), 2387–2425.
15 Z. H. Wang, Y. Y. Chang, J. G. Wu, C. Y. Lin, H. L. An, S. C. Luo, T. K. Tang and W. F. Su, *Macromol. Biosci.*, 2018, **18**(3), 1700251.
16 Z. Song, Z. Han, S. Lv, C. Chen, L. Chen, L. Yin and J. Cheng, *Chem. Soc. Rev.*, 2017, **46**(21), 6570–6599.
17 M. Rad-Malekshahi, L. Lempsink, M. Amidi, W. E. Hennink and E. Mastrobattista, *Bioconjugate Chem.*, 2016, **27**(1), 3–18.
18 K. Numata, *Polym. J.*, 2015, **47**(8), 537–545.
19 C. Y. Lin, S. C. Luo, J. S. Yu, T. C. Chen and W. F. Su, *ACS Appl. Bio Mater.*, 2019, **2**(1), 518–526.
20 G. A. Silva, C. Czeisler, K. L. Niece, E. Beniash, D. A. Harrington, J. A. Kessler and S. I. Stupp, *Science*, 2004, **303**(5662), 1352–1355.
21 C. Y. Brazel, J. L. Nunez, Z. Yang and S. W. Levison, *Neuroscience*, 2005, **131**(1), 55–65.
22 M. Takeda, A. Takamiya, J. W. Jiao, K. S. Cho, S. G. Trevino, T. Matsuda and D. F. Chen, *Invest. Ophthalmol. Vis. Sci.*, 2008, **49**(3), 1142–1150.
23 T. C. Chen, P. Y. She, D. F. Chen, J. H. Lu, C. H. Yang, D. S. Huang, P. Y. Chen, C. Y. Lu, K. S. Cho, H. F. Chen and W. F. Su, *Int. J. Mol. Sci.*, 2019, **20**(1), 178.
24 T. K. Dash and V. B. Konkimalla, *J. Controlled Release*, 2012, **158**(1), 15–33.
25 Y. Okada, T. Sumioka, K. Ichikawa, H. Sano, A. Nambu, K. Kobayashi, K. Uchida, Y. Suzuki, M. Tominaga, P. S. Reinach, S. I. Hirai, J. V. Jester, M. Miyajima, K. Shirai, H. Iwanishi, W. W. Kao, C. Y. Liu and S. Saika, *Lab. Invest.*, 2019, **99**(2), 210–230.
26 P. H. Chen, H. C. Liao, S. H. Hsu, R. S. Chen, M. C. Wu, Y. F. Yang, C. C. Wu, M. H. Chen and W. F. Su, *RSC Adv.*, 2015, **5**, 6932–6939.
27 T. L. Ma, C. M. Tsai, S. C. Luo, W. L. Chen, Y. C. Huang and W. F. Su, *React. Funct. Polym.*, 2022, **175**, 105265.
28 S. Sigelman and J. S. Friedenwald, *AMA Arch. Ophthalmol.*, 1954, **52**(1), 46–57.
29 R. W. Beuerman and B. Schimmelpfennig, *Exp. Neurol.*, 1980, **69**(1), 196–201.
30 K. Araki, Y. Ohashi, S. Kinoshita, K. Hayashi, Y. Kuwayama and Y. Tano, *Curr. Eye Res.*, 1994, **13**(3), 203–211.
31 J. P. Gilbard and S. R. Rossi, *Ophthalmology*, 1990, **97**(3), 308–312.
32 H. S. Dua, D. G. Said, E. M. Messmer, M. Rolando, J. M. Benitez-Del-Castillo, P. N. Hossain, A. J. Shortt, G. Geerling, M. Nubile, F. C. Figueiredo, S. Rauz, L. Mastropasqua, P. Rama and C. Baudouin, *Prog. Retinal Eye Res.*, 2018, **66**, 107–131.
33 L. You, F. E. Kruse and H. E. Volcker, *Invest. Ophthalmol. Visual Sci.*, 2000, **41**(3), 692–702.
34 E. Kijenska-Gawronska, T. Bolek, M. Bil and W. Swieszkowski, *J. Mater. Chem. B*, 2019, **7**(29), 4509–4519.
35 F. Lin, X. Y. Wang, Y. Y. Wang, Y. S. Yang and Y. Li, *Rsc. Adv.*, 2017, **7**(66), 41593–41602.
36 M. A. Alvarez-Perez, V. Guarino, V. Cirillo and L. Ambrosio, *Biomacromolecules*, 2010, **11**(9), 2238–2246.
37 C. Yang, W. Huang, L. Chen, N. Liang, H. Wang, J. Lu, X. Wang and T. Wang, *J. Mater. Chem. B*, 2021, **9**(3), 567–584.
38 J. A. Apablaza, M. F. Lezcano, A. Lopez Marquez, K. Godoy Sánchez, G. H. Oporto and F. J. Dias, *Polymers*, 2021, **13**(15), 2563.
39 A. Baradaran-Rafii, E. Biazar and S. Heidari-Keshel, *ASAIO J.*, 2015, **61**(5), 605–612.
40 B. Kong, W. Sun, G. Chen, S. Tang, M. Li, Z. Shao and S. Mi, *Sci. Rep.*, 2017, **7**(1), 970.
41 M. Himmler, F. Garreis, F. Paulsen, D. W. Schubert and T. A. Fuchsluger, *Sci. Rep.*, 2021, **11**(1), 18858.
42 J. I. Kim, J. Y. Kim and C. H. Park, *Sci. Rep.*, 2018, **8**(1), 3424.
43 S. Omer and R. Zelko, *Pharmaceutics*, 2021, **13**(10), 1637.